Ultra-Low Power Schottky Barrier TFT-Based Neurotransmitter Detection and Regenerative Studies

Abhijeet Barua, Ryan J. White, Kevin D. Leedy, Vidya Chidambaran, and Rashmi Jha

***Abstract*—There is limited work on understanding Schottky barrier (SB) field-effect transistor (FET) behavior, and subsequent evolution of sensitivity metrics under wet detection conditions for neurotransmitter sensing applications. In this work, we report low-power deep subthreshold (DST) characteristics of SB $InGaZnO_4$ (IGZO) thin film transistors (TFTs) and implement this regime for sensitive and selective *ex vivo* detection of Dopamine against Adenosine Triphosphate (ATP). Device regeneration was performed under liquid solution environment over 34 days and sensor response was observed to drift less than two orders of magnitude. Nevertheless, the quantified trends due to buffer solution baseline versus target conjugation were virtually preserved across the TFTs. Widely improved detection metrics were extracted from the detection tests, namely the limit of detection (LoD) in the 100fM-100pM range, a binding affinity (k_D) between 2.03×10^{-11}-3.02×10^{-9}M limits, and high sensitivity around 31-42mV/decade of target concentration. Although a steady drift with clear, repeatable differences between the device state at the start and end of the 34-day period were obtained, these devices were functional even after the regeneration test period. Such results can be used to estimate the regenerative lifetime of TFT biosensors under aptamer-immobilized solution environment detection conditions.**

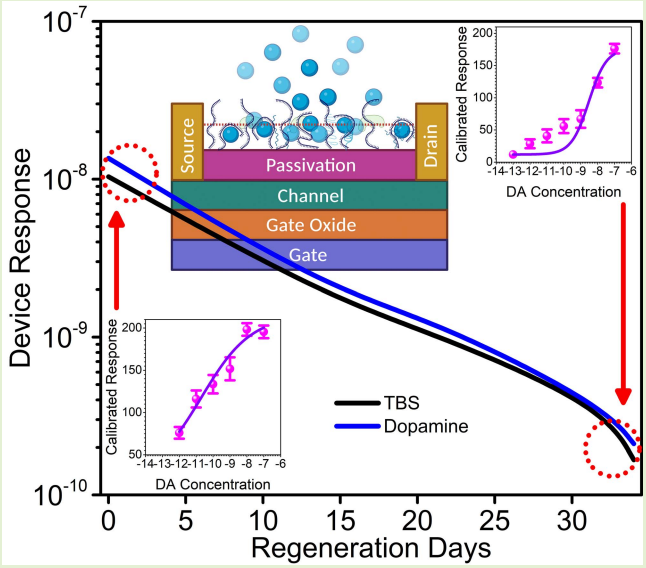

***Index Terms*—Biosensor, thin film transistor, IGZO, aptamer, dopamine, detection, drift, regeneration.**

I. Introduction

TO UNDERSTAND the evolution of brain functions in the context of patterns in neuronal activity and their correlation to complex behavior, it is imperative that next-generation sensors with high accuracy, multiplexed operation, multi analyte detection capabilities with ultra-sensitive and ultra-selective features are developed in a non-destructive, non-invasive or minimally-invasive manner such that they find applications in point-of-care platforms, diagnostics research, biomedical/healthcare industry, behavioral modeling, and wearable technology domain [1]–[6]. Therefore, it is important to quantify spatial and temporal neurotransmitter dynamics in real-time to explore their influence on neuromodulation of brain and body functions, on stimuli response, and on processing information, whether in serum, plasma, sweat, or urine. One of the major neurotransmitters, Dopamine is a catecholamine with the chemical name 2-(3,4-dihydroxyphenyl) ethylamine. It plays a crucial role in brain functions, renal system, hormonal functions, motor functions, and in the cardiovascular system. Within the central nervous system, Dopamine controls neuroendocrine and cognitive functions. The clinical concentration of Dopamine varies in the 100pM-1nM range within the blood-brain barrier, whereas in the 10pM-1mM range in serum and/or plasma. Dynamic or long-term imbalances in such concentration

Manuscript received February 9, 2022; accepted February 28, 2022. Date of publication March 4, 2022; date of current version April 14, 2022. This work was supported by the National Science Foundation (NSF) under Grant CNS-1556301, Grant SHF-1718428, Grant ECCS-1926465, and Grant ECCS-2128685. The associate editor coordinating the review of this article and approving it for publication was Prof. Yu-Cheng Lin. *(Corresponding author: Abhijeet Barua.)*

Abhijeet Barua and Rashmi Jha are with the Department of Electrical Engineering and Computer Science, University of Cincinnati, Cincinnati, OH 45220 USA (e-mail: baruaat@mail.uc.edu; jhari@ucmail.uc.edu).

Ryan J. White is with the Department of Electrical Engineering and Computer Science and the Department of Chemistry, University of Cincinnati, Cincinnati, OH 45220 USA (e-mail: white2r2@ucmail.uc.edu).

Kevin D. Leedy is with the Sensors Directorate, Air Force Research Laboratories, Wright Patterson Air Force Base, Dayton, OH 45433 USA (e-mail: kevin.leedy@us.af.mil).

Vidya Chidambaran is with the Cincinnati Children's Hospital Medical Center, Department of Anesthesia and the Department of Anesthesia and Pediatrics, University of Cincinnati, Cincinnati, OH 45229 USA (e-mail: vidya.chidambaran@cchmc.org).

This article has supplementary downloadable material available at https://doi.org/10.1109/JSEN.2022.3156883, provided by the authors.

Digital Object Identifier 10.1109/JSEN.2022.3156883

ranges may lead to mainly neurodegenerative disorders and psychiatric conditions such as Schizophrenia, Alzheimer's, Parkinson's disease, etc. Dysfunction of the mesolimbic dopaminergic system (Dopamine-DARPP32, PARK16, DRD4, COMT) has been implicated in chronic pain, depression, and opioid abuse as it plays salient roles in reward-risk behavior [7]–[10].

Purely electronic devices such as field effect transistors (FET) can reveal a change in transconduction due to the presence of target modified charged or uncharged aptamer motifs on channel surface, where the added advantage is one of amplification, and in turn higher sensitivity to dynamic changes in real-time as well as low power operation and integration with flexible substrates. To have a holistic understanding of genomics, expression studies and proteomics are essential, and it is anticipated that FET platforms can in the future enable the analysis of quantitative and relative changes in Dopamine concentrations in animal and human brains. Such properties can be incorporated through amorphous oxide semiconductors like $InGaZnO_4$ (IGZO). The reason for the prominence of IGZO in display technology and its foray into other disciplines can be primarily attributed to the requirement of spherically symmetric conduction bands with large ionic radius which allow efficient carrier transport and circumvents the condition for organized lattice or long-range order. This in turn scales down the thermal budget for the development of such films. The simplest form for the above criteria are *ns* orbitals which are predominantly found in cations from Group 12 and 13 of the periodic table. Within this group, In, Ga, and Zn have high incidence of binary oxide formation, which means that each of their cationic effects can be isolated and analyzed (details in SI). Therefore, IGZO films exhibit conventional CMOS process complexity, lower than CMOS thermal budgets, good structural flexibility, low leakage due to the wide bandgap, high mobility due to primary *ns* orbital transport, and threshold voltage stability [11]–[17].

IGZO thin film transistors (TFTs) mainly find applications in display circuits and therefore their original motivation was high drive current. For this reason, they were explored at near-threshold or above-threshold operational regions with equivalent high biases and Ohmic contacts. In above threshold region, the high voltage biases restrict low power operation and hence it is incompatible with wearable integration. When it comes to biosensor applications, noise immunity and low-power operation are more important. It is true that conventional FETs can be operated in the subthreshold regime and allow higher sensitivity due to the power dependency of the drain current on the gate voltage and the subthreshold slope with modulation from perturbations of the recognition elements after target conjugation [18], [19]. However, in the subthreshold regime, although unity voltage operation is theoretically possible, it comes at the cost of inhibited FET output resistance (r_0) due to the non-flat profile of output trends in saturation and hence limited intrinsic gain (A_i).

Low intrinsic gain leads to low sensitivity due to low resolution of amplification of target conjugation signals. In this context, a deep subthreshold regime (DST) at low voltage biases can be easily extracted for Schottky barrier (SB) TFTs due to the predominance of metal-semiconductor (M-S) barriers which dictate the field emission and thermal emission transport at such low biases rather than the channel resistance. The channel resistance for SB-TFTs only comes into action when the Schottky barrier is overwhelmed by the threshold or above-threshold operation points. Due to this modulation of the barrier height even at low operation points of $V_{DS} = 200mV$ and $V_{GS} = 500mV$ in our devices, the output resistance (r_0) became virtually independent of the drain-source bias and was a function of only the gate bias. By its almost flat profile in saturation, r_0 magnitudes were higher than conventional FETs, which led to a higher intrinsic gain factor A_i [20]. Since the above operation points are also applicable when the TFTs are used as biosensors, therefore at such small operation points and drive currents, any nanoscopic perturbance on the active surface tends to manifest as an incremental change in the current signal such that standby power consumption is given by $I_{off} \times V_{DD} \approx$ 1-100nW and hence the ultra-low power is ascribed to this characteristic. CMOS voltage operational points currently remain in the 0.9V-1V regime and hence we aimed to define our detection strategy within this range to promote CMOS logic compatible unity voltage ($\leq$1V) and ultralow power operation.

Recently, SB-IGZO-TFTs operated in DST have been reported as biosensors for Dopamine detection [13], [21]. Here, the presence of a source side Schottky barrier and depletion region in reverse bias, modulated by the gate bias, facilitates carrier injection or extraction which predominantly controls the carrier transport across the M-S interface. Though these initial findings are promising, any biosensor in contact with relevant tissues or fluids *in vivo* will demonstrate a drift in performance over time due to slow surface reaction with the tissue or fluid electrolytes, especially H species. This raises question about the reliability and operation of FET based sensors in liquid environments. Therefore, it is our endeavor to quantify such drift and regeneration capabilities over a period of time of the order of days instead of a general evaluation over hours or minutes [22], [23]. A detailed understanding in this area will help design of peripheral circuits with adequate tolerances such that detection metrics remain within a satisfactory range. Such an evaluation would allow the design of readout circuitry which are drift-aware with necessary calibration. In this paper, we first report the performance of SiO_2 passivated SB-IGZO TFT as a Dopamine sensor with high sensitivity and selectivity. Then, we perform short term ($\approx$34 days) device regeneration studies with accompanied drift under the presence of aptamer surface modification "click" chemistry to evaluate the change in metrics of limit of detection (LoD), sensitivity (Hill slope), maximum saturation signal (S_{max}), and binding affinity (k_D). These studies provide a comprehensive understanding on the changes and drifts in the device behavior in pristine and under solution environment aptamer-target conjugation conditions for acceptable biosensor operation.

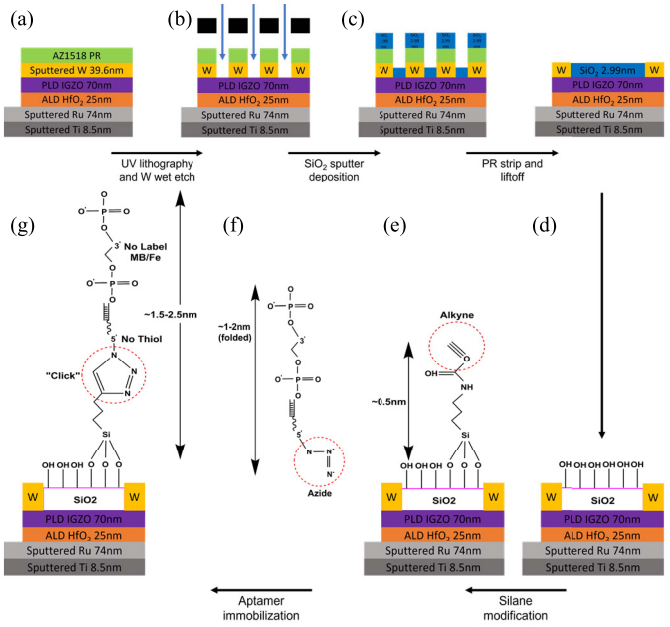

Fig. 1. (a) Devices after deposition of W top electrode to form source/drain contacts. (b) Patterned devices after UV lithography, development, and W wet etch. (c) Sputter deposition of 2.99nm of SiO_2 as the passivation layer on top of patterned areas. (d) Presence of hydroxyl (-OH) bonds on SiO_2 after deposition, PR strip, and liftoff. (e) Alkyne terminated carbamate silane modified surface. (f) "Click" chemistry reaction between silane terminal alkyne and azide modified Dopamine aptamer. (g) Before detection aptamer immobilized passivation layer surface.

II. Materials and Methods

A. Schottky TFT Fabrication

The TFTs were fabricated on a 4-inch p-Si/SiO_2 substrate with a bottom gated, inverted staggered topology (Fig. 1(a-d)). Room temperature (RT) radio frequency (RF) magnetron sputter process was used to deposit adhesion promoter Ti and bottom gate Ru *in situ* with no chamber vacuum break in an Ar gas environment. Thereafter, amorphous HfO_2 film with short range order was deposited at 250°C as the high-k dielectric through atomic layer deposition (ALD). This was the maximum temperature used in the entire fabrication flow. The precursors were Tetrakis(dimethylamido)hafnium (IV) ($Hf[N(CH_3)_2]_4$) as the Hf source and remote RF O_2 plasma as the oxygen source. A 50mm (2") diameter, 6mm thick sintered ceramic disk of In_2O_3:Ga_2O_3:ZnO with a 1:1:5 molar ratio was used to deposit stoichiometric $InGaZnO_4$ layer on top of the HfO_2 film through pulsed laser deposition (PLD) at 25°C. A post IGZO deposition anneal was performed at 200°C in air ambient for 30mins to recover device properties, repair any damaged tracks in the layers, and to improve the IGZO/HfO_2 interface. Top electrode W was deposited through sputter process and the TFTs were patterned into active regions through UV photolithography. The devices had mask dimensions of W/L=1300μm/200μm. Channel passivation layer (PL) SiO_2 was sputtered on the patterned wafer after W was wet etched from active channel areas, whereas the source/drain W areas were still protected by the positive photoresist which formed a soft mask for SiO_2.

B. Surface Modification and Aptamer Immobilization

The hydroxylated surfaces were treated chemically via undiluted Silane coupling agent 90% O-(Propargyl)-N-(Triethoxysilylpropyl) Carbamate with an alkyne termination group which was drop casted on the devices laid in a petridish for overnight reaction of approximately 16hours to prepare alkyne-terminated SiO_2 hybrid interfaces. It is a trialkoxy silane with olefin functional group that belongs to the organoethoxysilane chemical family. The hydroxyl-terminated SiO_2 surface associates through covalent Si-O bonds to bind the hydrolyzable group such that the 57-nucleotide 1μM Dopamine DNA oligonucleotide with a 5' azide (NHS Ester) modification can attach to the alkyne anchor (5' – Azide – GT CTC TGT GTG CGC CAG AGA CAC TGG GGC AGA TAT GGG CCA GCA CAG AAT GAG GCC C – 3'). Thereafter, ethanol and DI water was used to clean the surface. For the "click" reaction on SiO_2 surface, coarse amorphous powder Cu(I)Br was used as the catalyst. A calculated amount of Cu(I)Br crystal was added in a volumetric flask to 5mL of 20mM TBS and vortexed for 1min to produce a 10 mM strength of aptamer buffer solution (Cu(I)Br+TBS solution). The Dopamine aptamer stock aliquots (2μL) were centrifuged for 15s at 10000rpm. A 1000-fold dilution was used to reduce the 200uM (0.2mM) aptamer stock to concentrations of 200nM for aptamer immobilization. This was performed through the mixture of the entire 2uL 200uM aptamer stock aliquot with 2mL 10mM Cu(I)Br + TBS solution as prepared above and then vortexed for 1min. This final Dopamine aptamer + Cu(I)Br + TBS solution was finally placed on silanized devices at room ambient temperature (Fig. 1(e-g)). Different incubation times were tried between 10mins to 18hours, and the best stable data was observed from devices with 10mins incubation. Hence, for the rest of the experiments, 10minutes was fixed as the standard incubation time. This was followed by a DI water rinse and N_2 dry.

C. Target Preparation

ATP disodium salt target (Molecular weight 551.14g/mol) was dissolved in 8mL 20mM (0.1X) TBS buffer and a final concentration of 100mM was obtained after addition of crushed NaOH pellets and DI water to bring the pH to 7.4 and final volume to 10mL. Thereafter, the ATP target was serially diluted to 10nM/100 nM concentrations. Photo-unstable Dopamine target could be prepared only before target conjugation to aptamers for detection studies. For this, 12.1M original HCl solution was diluted to 100mL 0.1M HCl solution final volume in DI water and vortexed for 1min. Dopamine activation was achieved through dissolution of synthetic Dopamine hydrochloride in the 0.1M HCl (pH$\sim$1.14). For this, Dopamine hydrochloride (Molecular weight 189.64g/mol) was dissolved in 20mL 0.1M HCl solution prepared above and vortexed to produce a 1mM stock concentration of Dopamine target. Multiple target concentrations from 100fM to 100nM were then prepared for target detection in 0.1X$\approx$20mM TBS through serial dilution.

III. Results and Discussion

A. Pristine Deep Subthreshold Behavior

The devices were electrically characterized under ambient environment at RT of 298K in a Cascade Microtech MPS150 Probe Station with a Keithley 4200A Semiconductor Characterization System (SCS). Factors such as channel carrier density, passivation of oxygen vacancies in the channel, diffusion/drift mechanism, architecture, and work function of the metal electrode dictate the charge carrier injection or extraction across a junction composed of a metal-semiconductor-metal (M-S-M) [20], [21], [24], [25]. Traditionally, low resistance Ohmic or bad Schottky contacts, are formed from metals which have a low work function and form a low M-S barrier profile hypothetically. In channel oxides with carrier concentrations in semiconducting regimes ($\leq 10^{16}$cm^{-3} carrier density), such low barriers enable high conductance, high mobility, and linear behavior. However, in higher carrier concentrations ($\geq 10^{17}$cm^{-3} carrier density), this can cause loss of switching control, non-modulation of device behavior with gate bias, increased gate leakage, and increased off current in TFT operation. In such cases, high barrier Schottky contacts can be used instead to tightly modulate channel conduction due to a higher series drift resistance that induces rectifying non-linear behavior and suppresses leakage. Particularly in a positive quadrant operation, the source side Schottky barrier limits the emission current in the deep subthreshold and subthreshold regime, whereas in the above threshold or "on" state, this barrier effect is transparent to carrier flow because of the channel resistance dominance.

Due to such manifestation in device characteristics only at below threshold operation, Schottky barrier TFTs in this study have been demonstrated to operate at low voltage biases ($\leq$1V) in the deep subthreshold regime (near "off" state) such that their standby power consumption given by $I_{off} \times V_{DD}$ is low ($\approx$1nW). In case of amorphous oxide semiconductors (AOSs), the presence of electron rich cationic *ns* orbitals and electron deficient oxygen *np* orbitals lead to an interesting hybridization that occurs when these two species are brought together within the amorphous microstructure as shown in Fig. 2(a). Under normal oxygen deposition environments or removal of oxygen post-deposition, there are fewer unbonded oxygen present that leads to oxygen vacancies (V_O) whereas the electron rich cations In, Ga, and Zn tend to donate their electrons to the hybridized orbitals to achieve a lower energy state, and hence become conduction electrons when they create such shallow donor levels. Such vacancy content in a film is qualitatively related to the lattice bound oxygen percentage sans the interstitially bound oxygen. Therefore, it can be a measure of the free carrier concentration in an AOS. Hence, the passivation of vacancies and reduction in channel carrier density go hand in hand. There seems to be an inverse relation between increase of oxygen partial pressure on deposition or thermal treatments in oxygen ambient, and a decrease in the V_O levels with a corresponding decrease in the carrier concentration.

Consequently, there are two main approaches to form the non-ideal Schottky interface at the source/drain M-S contacts. First would be to bring the carrier concentration to semiconducting levels through oxygen partial pressure adjustment at the deposition stage itself or after-deposition or after-fabrication thermal treatment to alter the oxygen vacancies [15], [26], [27]. Second would be to use a semiconductor with a work function (and electron affinity) that is sufficiently different from the metal work function and therefore can form Schottky barriers at the M-S-M junctions without any change of deposition or thermal conditions. Furthermore, from previous studies, it has been inferred that as carrier concentration increases, the barrier height decreases under constant molar and atomic target compositions. Similarly, barrier height has a direct dependency on temperature through the well-known diode current relation. The molar stoichiometry as such can be adjusted by adjustment of partial pressure of oxygen in deposition, and therefore there is a direct linear correlation between oxygen and barrier height.

From ideal heterostructure band analysis, we determined that W as source/drain metal would theoretically provide a built-in barrier height of $\approx$0.35eV at the metal-semiconductor junction [13]. This is theoretically above the Ohmic contact ceiling and could play a role in the quasi-Schottky rectification of the devices. However, we observed a higher experimental zero bias barrier height $q\varphi_{B0} \approx 0.531$eV as the two materials were brought into contact such that there was movement of majority carriers from one material to another due to the equalization of Fermi levels based on discrepancy of their individual work functions (electron affinity in case of the semiconductor). Therefore, a barrier is created at the M-S interface that impedes the carrier transport. Charged interface states within the semiconductor bandgap may be created due to the abrupt chemical termination of the semiconductor lattice against the metal. Such metal-induced gap states (MIGS) may be occupied by majority carriers that effectively lead to the pinning of the bandgap center to the Fermi level and as such, the barrier height has negligible dependence on the work function of either material, in contrast to the Schottky barrier definition, and hence the higher observed initial value above. Fortunately, the pinned Fermi level at the M-S interface showed an experimental dependence on the bottom gate bias and a clear barrier lowering was observed across device characteristics with incremental gate steps.

The qualitative behavior of metal-semiconductor junctions at the source and drain can be evaluated by a sweep on one terminal and the other terminal remains grounded. From Fig. 2(b), a rectifying behavior is observed in the linear current-voltage data of the M-S-M diodes with a floating gate as well as stepped gate bias. The main contributor to this charge transport is the highly resistive semiconductor channel. For an *n*-channel, under positive applied bias, the predominant limitation on current emission is the reverse biased Schottky diode on the source side. An effective ideality factor of 1.0014 was extracted from the reverse biased Schottky trend. The ideality factor seems reasonable given the fact that such values remain between 1-1.2 for Schottky diodes and >1.2 for *pn* junction diodes. For the output IV plot, at an extremely low bias on the drain terminal, the Schottky diode on the drain side transitions from equilibrium to a forward bias that governs the leakage and quasi-linear/quasi-Schottky

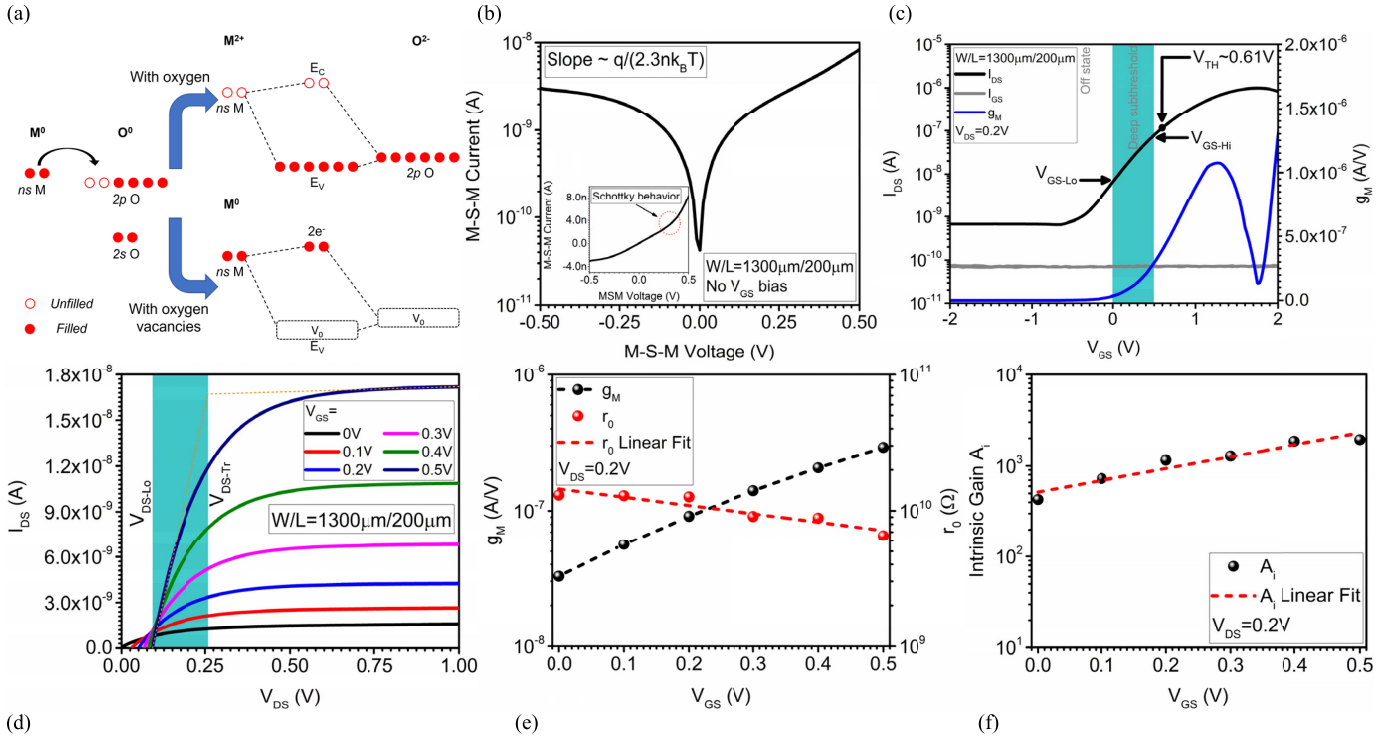

Fig. 2. (a) Hybridization of *ns* (from metal M: In, Ga, Zn) and *np* orbitals (from oxygen O) in IGZO to form the shallow donor levels in the presence of oxygen vacancies to provide conduction electrons for channel transport. Conduction electrons are scarcely available with the passivation of oxygen vacancies. (b) M–S–M IV trends that show the Schottky nature of the barrier and the same in linear scale (inset). (c) Transfer characteristics at V_{DS} = 0.2V wherein a deep subthreshold regime with low gate leakage next to the OFF state was extracted. (d) Output behavior within the deep subthreshold regime ($V_{GS\text{-}Lo}$ to $V_{GS\text{-}Hi}$) to obtain the output conductance and resistance for intrinsic gain determination. (e) Complementary transconductance (g_m) and output resistance (r_0) behavior used to extract device intrinsic gain A_i. (f) Stable intrinsic gain nearly two orders of magnitude higher than ohmic IGZO TFTs for the deep subthreshold region of operation.

transport respectively. At some point, a larger drain bias firmly establishes the forward biased drain Schottky diode, in which case, the source becomes reverse biased and governs the entire channel transport whereas drift phenomenon governs the drain carrier collection. Thus, at any given V_{GS}, the channel current is dominated primarily by the reverse saturation emission current of this source diode. Therefore, with a positive sweep of drain bias and fixed gate bias, there is a gradual transition of the drain barrier limitation to a source limitation until the Schottky barrier on the source side definitively dominates and saturates the channel transport. Gate bias steps modulate this source Schottky barrier through a lowering of the barrier height to increase thermionic emission relative to thermionic field emission or quantum mechanical tunneling across the M-S junction, because of which the devices show earlier current saturation with flatter output curvature profiles. This yields a higher intrinsic gain that is important for high sensitivity.

To enable unity voltage operation, a deep subthreshold region between 1nA and 100nA near the OFF state was defined from the transfer characteristics (Fig. 2(c)) such that the gate voltage limits were extracted as $V_{GS\text{-}Lo} = 0V$ and $V_{GS\text{-}Hi} = 0.5V$ for this deep subthreshold region. Hence under biosensor wet tests, these limits along with a drain bias of 0.2V would signify the upper and lower bounds of the high intrinsic gain unity voltage operation. The objective is to design the operation point of the biosensor TFTs specifically inside these bounds to incorporate the amplification attributed to MOSFET devices. Although a 25nm thin HfO_2 insulator layer should lower tunneling probability to limit the gate leakage to very small ranges (<1pA as achieved in our unpassivated devices), we observed a higher <10pA leakage current across the device due to the formation of a leaky SiO_2 PL, which structurally and optically plays the role of channel protection, but comes at the cost of increased interface state density as evident from the total interface state density from these devices $\sim 6.65 \times 10^{13} cm^{-2} eV^{-1}$ compared to $3.72 \times 10^{12} cm^{-2} eV^{-1}$ from the unpassivated devices [21]. On translation to the gate bias steps in the output characteristics, early saturation was achieved inside this deep subthreshold regime, and at the highest stepped gate bias of 0.5V, the upper limit of drain to source transition voltage was around $V_{DS\text{-}Tr} \sim 0.28V$ (Fig. 2(d)). This can be used to define the operation of these biosensor TFTs in the output saturation region which implies the operation about unity voltages such that the measured signals in detection experiments remain stable with negligible drift. The two drain biases, one where the drain side barrier lowering allows a leakage to a quasi-Schottky barrier transport and another where this same transport changes from a quasi-Schottky to a saturation one due to the source side reverse bias limitation on the current, are $V_{DS\text{-}Lo}$ and $V_{DS\text{-}Tr}$.

Especially in the saturation region, at any increment beyond $V_{DS\text{-}Tr}$, almost flat characteristics were obtained that indicated higher than normal output resistance. There is negligible relative change in both $V_{DS\text{-}Lo}$ and $V_{DS\text{-}Tr}$ between $V_{GS\text{-}Lo}$ and

$V_{GS\text{-}Hi}$. The output resistance and transconductance obtained from the deep subthreshold regime at a drain bias of 0.2V (Fig. 2(e)) show complementary behavior with increase in gate bias. At $V_{DS} = 0.2$V, the intrinsic gain $A_i = g_m \times r_0$ was determined to be highly stable (∼1000) and the highest gain was obtained at gate voltage of 0.5V (Fig. 2(f)). In preliminary sampling at the noise floor and at $V_{GS} = 0.1$V, $V_{DS} = 0.2$V (not shown), devices exhibited high stability in the pristine state for approximately 20minutes, which strengthens the motivation for biosensor operation because in biomolecule detection, average temporal resolutions lie within this range. Hinged on the upper limit of the transition voltage $V_{DS\text{-}Tr} \sim 0.28$V, we chose the drain bias for uniform saturation operation as $V_{DS} = 0.2$V, and together with $V_{GS} = 0.5$V, can be defined for device operation to extract sensor metrics. Therefore, the operating point of the biosensors may be defined and selected according to the analysis above. In this way, the low drain bias ($\ll$1V) would not exceed the buffer solution electrochemical windows that are placed on the back channel. It should also prevent local work function change of the source/drain contacts under wet buffers and allow the device to be sampled at regular intervals with the target analyte for real-time analysis.

B. Target Detection

For a bottom gated design, the semiconductor back-channel may be exposed to subsequent source/drain etch process steps, illumination degradation as well as other ambient contaminants. Acceptor levels in the IGZO bandgap are provided by the conversion of $O_2(g) + e^- \rightarrow O^{2-}(s)$ from the surrounding oxygen on the back-channel surface and can push the device towards depletion mode operation whereas $H_2O(s) + h^+ \rightarrow H_2O^+(s)$ from moisture adsorbed from the environment may allow the predominant formation of surface hydroxyls (-OH) on the unpassivated back-channel and reinforces the enhancement mode operation of the *n*-type channel. To prevent such unwanted effects of ambient contamination, ingress of different environmental gases on the surface, and bias illumination instability, however without any protection from source/drain definition processes, back-channels are normally protected by an insulative PL such as SiO_x, Si_3N_4, HfO_x, Al_2O_3, organic polymers, etc. On the other hand, the Debye-Hückel length on top of the unpassivated surface allows closer proximity of the target biomolecules towards the back-channel which is amplified by an intrinsic gain of a purely electronic device such as a TFT and allows for improved detection metrics [6], [21]. Therefore, there could be a tradeoff between incorporation of back-channel/source/drain protection schemes and detection metrics of a bio-detection platform based on the quality and thickness of the protective layers.

To partially answer the above issues, we incorporated a back-channel PL SiO_2 on top of the IGZO layer through sputter deposition. The signals that arise from target-aptamer conjugation depends on a multitude of factors and for higher sensitivity, it is important that any surface areal event induces changes in some form on various electronic parameters in the channel, in this case the drain current. This may be possible through a better selection of surface recognition elements which are as close to ideal as possible (maximum surface coverage, zero non-specific binding, zero steric hindrance, maximum specificity, etc.). Alternatively, the device itself can intrinsically magnify any small signal if the inherent gain factor of the device is high such that the resolution is also improved. Since the calibrated response, and consequently the sensitivity of a biosensor is dependent on the amplification attributed to the electronic device, therefore SB-TFTs with a higher inherent amplification factor have a complimentary prospect of improved sensitivity. This supplements the use of SB-TFTs for biosensor applications. Additionally, SB-TFTs behave differently than conventional TFTs as they circumvent the need for weak inversion versus strong inversion in conventional devices and operate primarily through charge accumulation. For mass production purposes, traditionally doped source/drain requires accurate activation and drive-in process which is non-existent in metal-semiconductor based SB-TFTs with a straightforward low temperature process that bypasses the need to form operable Ohmic contacts and in effect precludes complex fabrication flow.

Electrical data was collected from the devices in the form of DC current-voltage (IV), capacitance-voltage (CV), and sampling behavior under pristine and under the influence of solution placed on the device surfaces within a polydimethylsiloxane (PDMS) well especially fabricated to define the exposure of SiO_2 PL to such non-physiological buffer and spiked analyte solutions. Additionally, the wells also prevented any crosstalk by isolating the action of the solutions on specific devices in comparison to other surface modified devices physically, although the inter-TFT distances were >5mm to begin with. As can be seen from Fig. 2(c), the gate leakage in relation to the transfer trends of the DC IV is extremely low in the range of a few pA and in addition to the 200mV bias on the drain side, presented another barrier to electrode fouling, operation beyond the electrochemical window of the buffer analyte solutions, and crosstalk.

The detection tests were performed in identical settings as the pristine device tests with a bottom gate top contact configuration and liquid solutions were placed within the PDMS wells, different from ion sensitive FETs (ISFETs) whereby an electrolyte gate is used to gate the channel directly through the electrolytic solution in the absence of an intrinsic device gate. Dopamine target-concentration dependent changes were observed in the transfer current of the devices across a wide range from 1pM to 100nM under the presence of 0.1X TBS buffer with different Dopamine concentrations which were placed on the surface with a volume of 2μL through a micropipette. These currents remained uniform through the entire gate sweep range as shown in Fig. 3(a) and to operate within the DST regime as defined in the previous section, a gate sweep range between 0 and 0.5V range with fixed drain bias of V_{DS} =0.2V was chosen and device behavior was extracted from this region as shown in Fig. 3(b).

Furthermore, to confirm the device conductance due to the channel and to preclude the contribution, if any, from the buffer solutions, another wafer was fabricated with an insulative material as the channel and tested to observe any

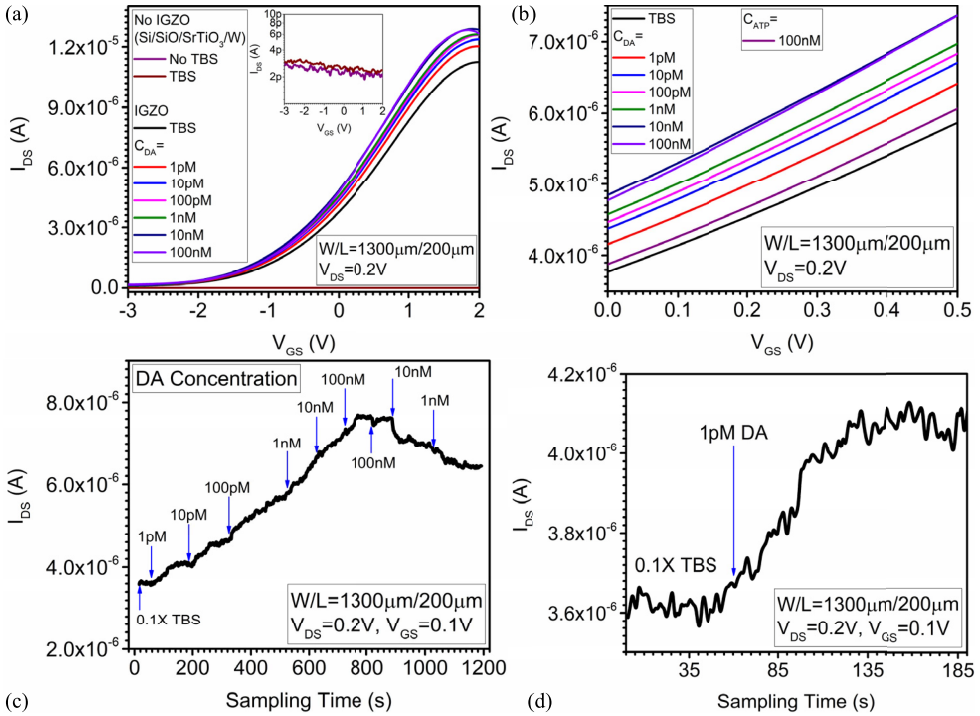

Fig. 3. (a) Preliminary changes in transfer current and transconductance dependent on Dopamine target-concentration measured against 0.1X TBS buffer as the baseline signal over the entire gate sweep range. Additionally, same sweeps were conducted under solution detection conditions across insulative $SrTiO_3$ channels with W S/D with uniform resistive behavior across the bias range in the pA current levels (inset) to confirm the carrier transport only through the IGZO channel. (b) Selective target-concentration dependent changes in S/D current in the DST regime for Dopamine in a linear increment from 1pM to 100nM against ATP at 100nM. (c) Real time cycling of Dopamine target-concentration that led to changes in sampling current across the time scale. (d) 0.1X TBS to 1pM DA evolution of real-time cycling signal to show a zoomed version of ligand binding to aptamer on channel surface and its diffusion time response.

conduction due to the buffer solutions or spiked target concentrations. Highly insulative $SrTiO_3$ was deposited on Si/SiO_2 wafers through sputter deposition under similar conditions and thickness as used for other channel depositions in this article, where the thermally oxidized SiO_2 acted as the gate dielectric, and 40nm W was deposited and patterned to form the source/drain electrodes. The $Si/SiO_2/SrTiO_3/W$ TFT devices were tested under pristine conditions and their behavior was found to be highly resistive as undoped $SrTiO_3$ behaves as an insulator. Moreover, the $SrTiO_3$ devices were immobilized in the same manner as described previously and thereafter tested under the same liquid environment as above where again they showed highly insulative behavior for 10nM and 100nM of Dopamine as can be seen in Fig. 3(a) and inset. This observation confirms that the channel conductance has negligible contribution from the ionic charge transfer in an electrolytic environment on top of the channel surface.

Initially, silanization leads to the hydrolysis of the three alkoxy groups which then undergo condensation and deprotonate the hydroxyl bonds present on the SiO_2 PL to form covalent bonds. Consequently, fewer H^+ ions are available on the PL surface to form a surface accumulation layer within IGZO, along with the fact that these ions are now at a farther distance from IGZO surface compared to no PL. On reaction with the azide-linked aptamer, the alkyne group from the silane reacts to form a 1,4-benzene isomer as shown in Fig. 1(g) such that the aptamer undertakes a folded primary spatial arrangement on top of the PL. The increase in channel conductance with fixed bias conditions but incremental target-concentration on aptamer immobilized IGZO TFTs points to the fact that upon target-aptamer conjugation, the aptamer undergoes a primary to secondary conformational rearrangement of its phosphodiester backbone which is primarily negatively charged. This rearrangement leads to an electrostatic charge redistribution through the buffer ions present in the solution, in the vicinity of the channel surface, or in this case, the SiO_2 PL. As this aptamer was specifically designed for Dopamine, the device response was tested against 100nM ATP which presented a minimal response compared to the highly selective Dopamine response.

It is pertinent to point out here that due to Debye screening beyond the Debye-Hückel length, it is ideal to have the bare semiconductor channel in direct exposure to the target analytes to enable highly sensitive detection of biomolecules. The addition of a PL on top of the active channel layer may lead to a tradeoff between improved channel protection and sensitive detection of analytes. Nonetheless, the target-induced signals are maximal from SiO_2 PL/IGZO TFTs compared to the $SrTiO_3$ devices. In this state of the device, given that Dopamine has a single positive charge and there is a progressive increase in the channel current trend lines with an increase in target-concentration, it can be hypothesized that the aptamers, in their secondary confirmational motif, spatially move farther away from the channel and thus orient

the backbone negative charges at a distance from the *n*-type carriers, which leads to a top-gating effect and allows more surface accumulation through the IGZO surface. Real-time cycling of different Dopamine concentrations was applied on the device surface in the sampling mode to qualitatively determine the time response and reproducibility (Fig. 3(c)).

Initially, TBS buffer was filled into the PDMS wells before the start of the test, and the response was allowed to stabilize for some time. This was considered as the response base trend for comparison against subsequent incremental and decremental target-concentrations which were spiked into the TBS buffer at successive time intervals. Device response increased with an increase in Dopamine concentration and decreased vice versa, with a lag time for the target to diffuse through the solution ions, in conjunction with the transfer response seen in Fig. 3(b) with similar current values. Non-saturation of some jumps could be due to the longer time required for the target to equilibrate in solution. In an ideal environment, non-specific binding should not occur on the active layer surface, but due to presence of some unpassivated voids in the PL, physico-chemisorption of ambient molecules, or surface radicals, such steric hindrance cannot be entirely negated and can play a role in the non-saturation of real-time response steps. The cycling test demonstrates the efficacy of the device to respond to rapid target-concentration changes and shows the stability of the devices across the entire sampling range. To further understand the temporal resolution, the jump from TBS baseline signal to 1pM Dopamine conjugation has been depicted in Fig. 3(d) where a step in the response is observed on target-aptamer conjugation, with response interval of several seconds, as the target diffuses through the electrolytic buffer ions to arrive at the surface.

C. Device Regeneration Under Solution Environment

Metal oxides, especially from the ZnO family, are known to chemically react with different pH solutions (particularly low acidic pH) under biosensor operation, to form electrolytic ions. It is important to understand the shelf life of these devices when exposed to repeated detection tests and for this purpose, a regeneration study was carried out. Across the lifetime of these devices, we expected a drift in device response due to the multiple immobilization trials performed on them, and since the detection signals are dependent on the channel transconductance, in turn a drift in the detection response as well. For this reason, we performed experiments where we subjected these devices to surface modification chemistry through a 34-day period and extracted sampling response under solution environment from the pure buffer as well as 10nM Dopamine target. The devices were regenerated by a standard clean process as described in the fabrication method by an extended solvent clean process that included Acetone, Methanol, and Isopropyl alcohol.

At each of these individual tests, the evolution of drift in these devices was quantified as shown in Fig. 4(a-e) with a regeneration of the sampling and DC IV response, with uniform and stable sampling response across the individual measurement, although the tendency was towards a lower current level over the total days. From Fig. 4f, it can be inferred that the detection response decreased by 98.67% over the original initial current response (from $\approx 1.5 \times 10^{-8}$A to 2×10^{-10}A) across which, the differences ($\Delta I = I_{DA10nM} - I_{TBS}$) between the TBS buffer and Dopamine response themselves tended to remain uniform, although some convergence can be seen around the 30-day mark, but fortunately, the devices still respond to target detection tests as of the preparation of this article, albeit at the reduced current levels. In the present state of these devices and at the close of the 34-day period, detection data has been presented in Fig. 5(a-d). This time, the transfer currents were obtained for a serial range between 100fM and 100nM with all other conditions identical as earlier (Fig. 5(a)). There were clear target-concentration dependent signal changes across the relevant devices. Similar trends in terms of increase of drain current values with increase in target-concentration were obtained.

In the real-time cycling tests shown in Fig. 5(b), a match with transfer current values from Fig. 5(a) can be seen, where the steps in response jumps are clearly observed for increments in Dopamine concentration. This could be attributed to the fact that since diffusion times were reduced due to multiple immobilizations, the targets could better equilibrate on the surface and lead to a saturation of responses. To evaluate the selectivity of these devices, 10nM ATP was also spiked into the PDMS wells and negligible response was obtained from the real-time response of the sensors. Even though the devices themselves settled to a high resistive state after rigorous immobilization trials over 34 days, their response still maintained distinction between different target-induced values and the TBS base trend. Around 100nM, in both the transfer curves as well as the sampling response, the current jumps towards a higher value, indicative of the start of non-specific binding on the surface. Due to reorientation of the negative DNA charges away from the surface, more electrostatic attraction occurs and greater participation of surface accumulation charges in the conduction process.

This change is reflected in parameters such as the threshold voltage, device transconductance, and obviously the on current, after ligand-binding. We mainly considered the transconductance (g_M) and the change in DST current at the operation point of $V_{GS} = 500$mV and $V_{DS} = 200$mV to extract a calibrated response which would be dependent on the capacitive coupling effect from the gate electrode bias, the carrier mobility or charge transport, and the geometry of the top surface (TFT dimensions), as follows:

$$Calibrated-response = \frac{I_{TBS} - I_{target}}{g_M} \Big|_{V_{GS} = 500mV,\, V_{DS} = 200mV}$$

This was individually done for each device and a mean calibration response could be extracted from the set of devices. The calibration responses were determined for initial wet detection tests as well as final ones and have been presented in Fig. 5(c-d). Hill function isotherms were used to fit the calibration dose responses and major detection metrics such as maximum saturation sensor signal (S_{max}), binding affinity (k_D), limit of detection (LoD), and detection sensitivity (Hill Slope) were obtained from the fits. In this regard, a clear distinction

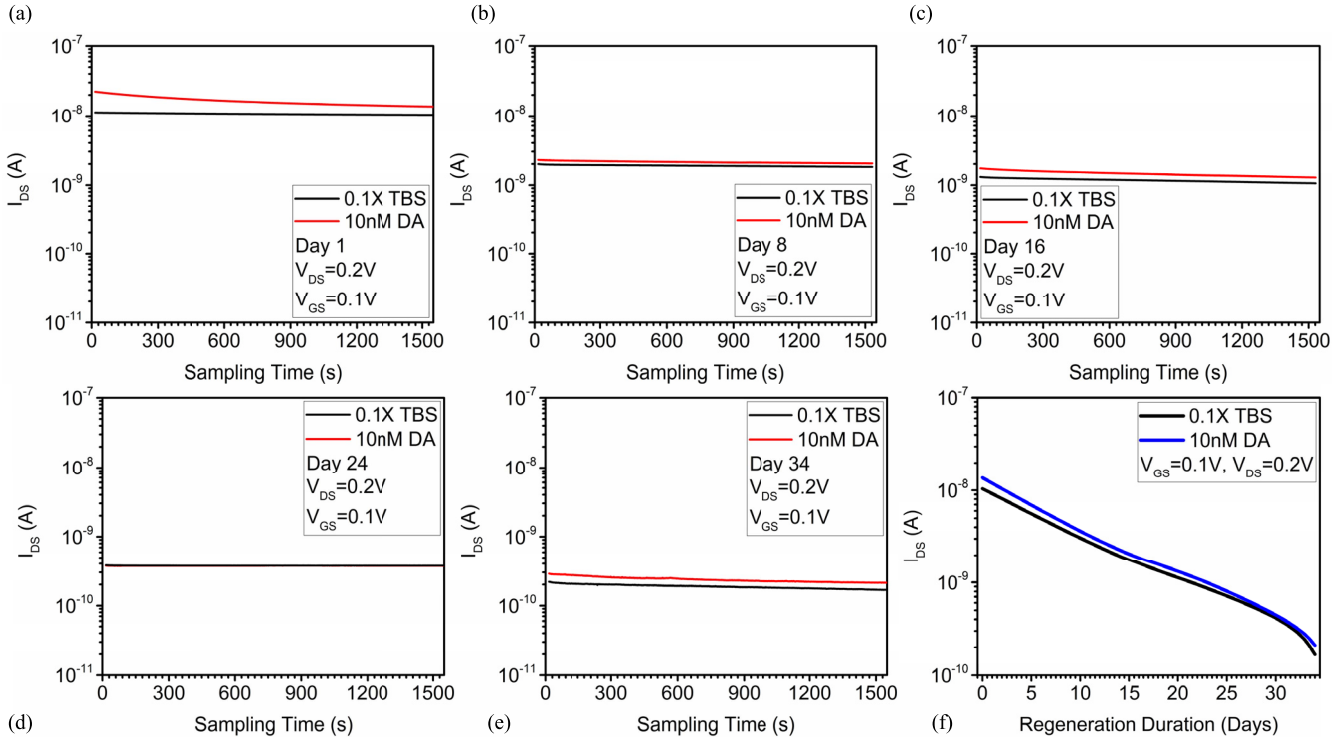

Fig. 4. (a-e) Multiple time point data of device regeneration for N=3 devices through 1, 8, 16, 24, 34 days when exposed to 10nM Dopamine target solution against 0.1X TBS buffer for fixed sampling bias across the TFT gate and drain. (f) Drift evolution of the device signal across 34 days through which the devices could be regenerated where the trends seem to converge as the regeneration tests approached 30 days. Devices are still functional as of September 2021.

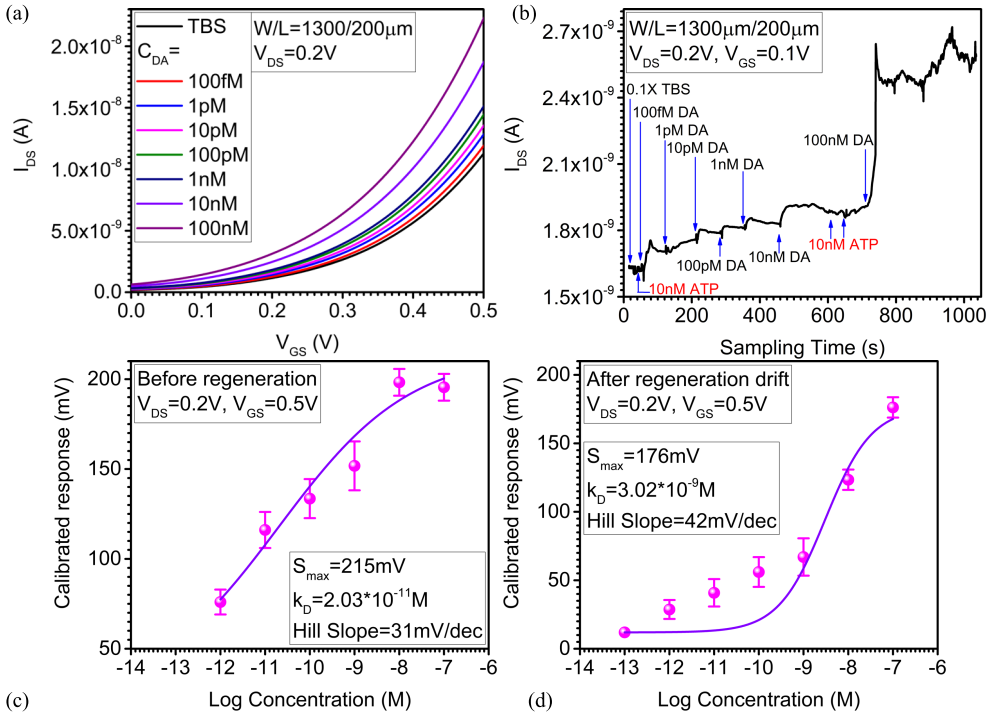

Fig. 5. (a) Transfer IV from DST regime with target-concentration dependent changes in the transconductance linearly from 100fM to 100nM at the end of the 34-day regeneration period. (b) Real-time cycling of target-concentrations against 0.1X TBS buffer to show incremental changes in sampling current due to Dopamine and negligible changes in current on equivalent addition of ATP to quantify selectivity of the devices. (c-d) Hill function isotherms fitted to the calibration response obtained from the devices before and after regeneration experiments to quantify detection metrics of saturation sensor response (S_{max}), binding affinity (k_D), limit of detection (LoD), and sensitivity (Hill slope).

can be observed from the detection responses between the initial and final tests. The initial calibration response has a higher maximum response than the final calibration isotherm, whereas the final calibration trend is right shifted compared

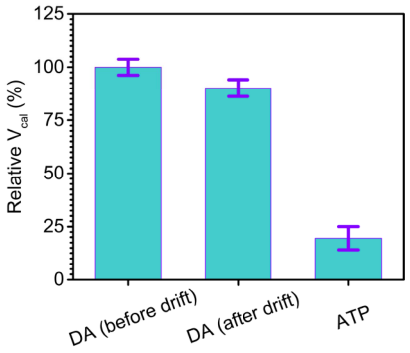

Fig. 6. Signal change after device drift from regeneration tests that show marginal change in calibration response to Dopamine compared to a minor change due to ATP.

to the initial calibration response. At the same time, the dose response fits produced a higher sensitivity for the right shifted final calibration response, whereas all other parameters are inferior to the initial response curve. Specifically, initially the detection metrics were an $S_{max} \approx 215$mV, $k_D \approx 2.03 \times 10^{-11}$M, a sensitivity of 31mV/decade of Dopamine concentration and an LoD between 100fM-1pM. Counterintuitively, the final dose response curve had a higher sensitivity of 42mV/decade of Dopamine concentration, whereas all other parameters such as $S_{max} \approx 176$mV, $k_D \approx 3.02 \times 10^{-9}$M, and LoD $\approx$ 100pM were secondary to the initial detection parameters.

In any case, their trends and values remain similar, and can be used to quantify the regenerative nature of such sensors through the evolution of drift in their electrical parameters over time. Therefore, Dopamine was successfully detected in a linear range between 100fM-100nM with reliable detection metrics. Such a range is sufficient for dopaminergic activity evaluation, whether *in vivo* or *ex vivo*. Finally, a comparison of relative calibration between initial Dopamine response, final Dopamine response and selectivity against ATP is depicted in Fig. 6, where signal change due to ATP is a minor fraction of Dopamine response, although it cannot be completely neglected. Such cross-reactivity has been reported for ATP as it is secreted by neurons with a regulatory function to inhibit glial cells around the dopaminergic synaptic space and has similar backbone.

Currently, the primary methods for real-time neurotransmitter detection comprise electrochemical techniques, optical methods, high performance liquid chromatography (HPLC)/mass spectroscopy (MS) through microdialysis, and nuclear imaging. Specifically, implantable electrochemical probes, positron emission tomography (PET), and magnetic resonance spectrometry (MRS) are used to analyze neurotransmitters *in vivo*. Typically, due to economic reasons, fast scan cyclic voltammetry (FSCV) and differential pulse voltammetry (DPV) are preferred over other methods. However, there is no CMOS compatible fabrication process or inherent amplification in electrochemical methods, along with the fact that at high scan rates, there is a non-practical amount of background current noise and due to the redox label nature, non-electroactive species are difficult to detect. Although there is drift over 34 days, the objective of this report is to reinforce the fact that even with such drift, the delta difference between buffer baseline signals and target-aptamer conjugation signals are preserved. Once such deviation is quantified, any peripheral readout circuitry can be calibrated to Fig. 4(f) at different time points through negative feedback to take advantage of the uniform delta and hence provide insightful information over the period of reliable biosensor operation.

IV. Conclusion

In summary, we used a minimal reagent, simple and facile 2-step chemistry to immobilize Dopamine-specific aptamers on SiO_2 passivation surfaces to provide a recognition element to identify and capture low concentrations of Dopamine target molecules. TFTs with PLD IGZO as the active semiconductor and sputtered SiO_2 as the top passivation layer were fabricated and their pristine solid-state characteristics were used to define a deep subthreshold regime of operation with specific choice of gate and drain biases, such that the Schottky related high intrinsic gain ($\geq$1000), only apparent in low operation voltage regions (unity voltage in this case), leads to improved calibrated responses and detection figures of merit. It should be noted that since channel passivation is different from source/drain protection layer, hence these devices, no matter how reliable, were expected to show some drift over short periods of regeneration time such as over a month. To quantify such device regeneration and drift, the devices were subjected to rigorous immobilization chemistry over a 34-day period and the detection metrics at the start and end of this period were LoD $\approx$100fM-100pM range, $k_D \approx 2.03\times10^{-11}$-$3.02\times10^{-9}$M limits, and sensitivity $\approx$31-42mV/decade of concentration. In this way, shelf life of such biosensors can be determined for commercial applications and can give an idea about sensor regeneration under different solution environment conditions. At the same time, future work is required to examine and evaluate the role of pH in the immobilization chemistry to further understand if it interferes with the active TFT layer on one end and target molecule on the other such that dependable operation of the sensor is preserved. Alternatively, other inorganic PLs such as Si_3N_4, SiN_x, HfO_x, etc. should be explored and validated for comparison of pristine device operation as well as detection metrics. In this regard, hydroxyl based surface tethers have been well studied. However, nitrogen rich surfaces may need the creation of an oxidation layer or silanol groups through oxygen plasma treatment or an alternative tether layer such as positive synthetic amino acid chain like Poly-L-Lysin (PLL) with amine or epoxide based functional groups on the 5' end of the aptamer such that it may react with the amino acid [28], [29].

Appendix

All supplementary results and figures are provided in the file "Supplementary Information".

Acknowledgment

Abhijeet Barua would like to thank Dr. Alisha Prasad, Hope Kumalki, Israel Belmonte, Vamshi Kiran Gogi,

Dr. Necati Kaval, Dr. Melodie A. Fickenscher, and Anuptha Pujari at the University of Cincinnati for useful discussions.

REFERENCES

[1] D. Sarkar, W. Liu, X. Xie, A. C. Anselmo, S. Mitragotri, and K. Banerjee, "MoS_2 field-effect transistor for next-generation label-free biosensors," *ACS Nano*, vol. 8, no. 4, pp. 3992–4003, Apr. 2014, doi: 10.1021/nn5009148.

[2] Y.-T. Li *et al.*, "Receptor-mediated field effect transistor biosensor for real-time monitoring of glutamate release from primary hippocampal neurons," *Anal. Chem.*, vol. 91, no. 13, pp. 8229–8236, Jul. 2019, doi: 10.1021/acs.analchem.9b00832.

[3] T. Sakata, "Biologically coupled gate field-effect transistors meet *in vitro* diagnostics," *ACS Omega*, vol. 4, no. 7, pp. 11852–11862, Jul. 2019, doi: 10.1021/acsomega.9b01629.

[4] G. Seo *et al.*, "Rapid detection of COVID-19 causative virus (SARS-CoV-2) in human nasopharyngeal swab specimens using field-effect transistor-based biosensor," *ACS Nano.*, vol. 14, no. 4, pp. 5135–5142, 2020, doi: 10.1021/acsnano.0c02823.

[5] S. Hong, S. P. Park, Y. Kim, B. H. Kang, J. W. Na, and H. J. Kim, "Low-temperature fabrication of an HfO_2 passivation layer for amorphous indium–gallium–zinc oxide thin film transistors using a solution process," *Sci. Rep.*, vol. 7, no. 1, p. 16265, Dec. 2017, doi: 10.1038/s41598-017-16585-x.

[6] A. Barua, T. H. Nguyen, Y. Wu, V. M. Jain, R. J. White, and R. Jha, "Ultrasensitive label-free tobramycin detection with aptamer-functionalized ZnO TFT biosensor," in *Proc. IEEE Nat. Aerosp. Electron. Conf. (NAECON)*, Jul. 2018, pp. 331–338, doi: 10.1109/NAECON.2018.8556707.

[7] V. Chidambaran *et al.*, "Enrichment of genomic pathways based on differential DNA methylation associated with chronic postsurgical pain and anxiety in children: A prospective, pilot study," *J. Pain*, vol. 20, no. 7, pp. 771–785, Jul. 2019, doi: 10.1016/j.jpain.2018.12.008.

[8] V. Chidambaran *et al.*, "Methylation quantitative trait locus analysis of chronic postsurgical pain uncovers epigenetic mediators of genetic risk," *Epigenomics*, vol. 13, no. 8, pp. 613–630, Apr. 2021, doi: 10.2217/epi-2020-0424.

[9] E. Navratilova, C. W. Atcherley, and F. Porreca, "Brain circuits encoding reward from pain relief," *Trends Neurosci.*, vol. 38, no. 11, pp. 741–750, Nov. 2015, doi: 10.1016/j.tins.2015.09.003.

[10] K. Zorina-Lichtenwalter, C. B. Meloto, S. Khoury, and L. Diatchenko, "Genetic predictors of human chronic pain conditions," *Neuroscience*, vol. 338, pp. 36–62, Dec. 2016, doi: 10.1016/j.neuroscience.2016.04.041.

[11] L.-Y. Su, H.-K. Lin, C.-C. Hung, and J. Huang, "Role of HfO_2/SiO_2 gate dielectric on the reduction of low-frequent noise and the enhancement of a-IGZO TFT electrical performance," *J. Display Technol.*, vol. 8, no. 12, pp. 695–698, Dec. 2012, doi: 10.1109/JDT.2012.2217728.

[12] A. Abliz *et al.*, "Enhanced reliability of In–Ga–ZnO thin-film transistors through design of dual passivation layers," *IEEE Trans. Electron Devices*, vol. 65, no. 7, pp. 2844–2849, Jul. 2018, doi: 10.1109/TED.2018.2836146.

[13] A. Barua, K. D. Leedy, and R. Jha, "Deep-subthreshold Schottky barrier IGZO TFT for ultra low-power applications," *Solid State Electron. Lett.*, vol. 2, pp. 59–66, Dec. 2020, doi: 10.1016/j.ssel.2020.10.001.

[14] S. Lee and A. Nathan, "Conduction threshold in accumulation-mode InGaZnO thin film transistors," *Sci. Rep.*, vol. 6, no. 1, p. 22567, Sep. 2016, doi: 10.1038/srep22567.

[15] T. T. Trinh, K. Jang, V. A. Dao, and J. Yi, "Effect of high conductivity amorphous InGaZnO active layer on the field effect mobility improvement of thin film transistors," *J. Appl. Phys.*, vol. 116, no. 21, Dec. 2014, Art. no. 214504, doi: 10.1063/1.4902856.

[16] J. Li *et al.*, "Effect of reactive sputtered SiO_x passivation layer on the stability of InGaZnO thin film transistors," *Vacuum*, vol. 86, no. 12, pp. 1840–1843, Jul. 2012, doi: 10.1016/j.vacuum.2012.04.009.

[17] T. T. Trinh, K. Jang, S. Velumani, V. A. Dao, and J. Yi, "Role of Schottky barrier height at source/drain contact for electrical improvement in high carrier concentration amorphous InGaZnO thin film transistors," *Mater. Sci. Semicond. Process.*, vol. 38, pp. 50–56, 2015, doi: 10.1016/j.mssp.2015.03.051.

[18] H. Nam *et al.*, "Multiple MoS_2 transistors for sensing molecule interaction kinetics," *Sci. Rep.*, vol. 5, no. 1, p. 10546, Sep. 2015, doi: 10.1038/srep10546.

[19] P. Georgiou and C. Toumazou, "ISFET characteristics in CMOS and their application to weak inversion operation," *Sens. Actuators B, Chem.*, vol. 143, no. 1, pp. 211–217, 2009, doi: 10.1016/j.snb.2009.09.018.

[20] S. Lee and A. Nathan, "Subthreshold Schottky-barrier thin-film transistors with ultralow power and high intrinsic gain," *Science*, vol. 354, pp. 302–304, Oct. 2016, doi: 10.1126/science.aah5035.

[21] A. Barua, R. J. White, K. D. Leedy, and R. Jha, "Ultra-low-power neurotransmitter sensor using novel 'click' chemistry aptamer-functionalized deep subthreshold Schottky barrier IGZO TFT," *MRS Commun.*, vol. 11, no. 3, pp. 233–243, Jun. 2021, doi: 10.1557/s43579-021-00028-w.

[22] C. G. Jakobson, M. Feinsod, and Y. Nemirovsky, "Low frequency noise and drift in ion sensitive field effect transistors," *Sens. Actuators B, Chem.*, vol. 68, nos. 1–3, pp. 134–139, Aug. 2000, doi: 10.1016/S0925-4005(00)00473-1.

[23] H. W. Son, M. Jeun, J. Choi, and K. H. Lee, "A strategy to minimize the sensing voltage drift error in a transistor biosensor with a nanoscale sensing gate," *Int. J. Nanomed.*, vol. 12, pp. 2951–2956, Apr. 2017, doi: 10.2147/IJN.S134441.

[24] L. E. Calvet, "Electrical transport in Schottky by barrier MOSFETs," Ph.D. dissertation, Yale Univ., New Haven, CT, USA, 2001, p. 1438 and 165, vol. 62-03.

[25] J. Troughton and D. Atkinson, "Amorphous InGaZnO and metal oxide semiconductor devices: An overview and current status," *J. Mater. Chem. C*, vol. 7, no. 40, pp. 12388–12414, Oct. 2019, doi: 10.1039/C9TC03933C.

[26] F. M. Hossain *et al.*, "Modeling and simulation of polycrystalline ZnO thin-film transistors," *J. Appl. Phys.*, vol. 94, no. 12, pp. 7768–7777, Oct. 2003, doi: 10.1063/1.1628834.

[27] J. M. Shannon and F. Balon, "Source-gated thin-film transistors," *Solid-State Electron.*, vol. 52, no. 3, pp. 449–454, Mar. 2008, doi: 10.1016/j.sse.2007.10.013.

[28] L. Reynaud, "Aptamer-functionalized nanopore for the detection of closely-related proteins," Dept. Biotechnol., Univ. Grenoble Alpes, Grenoble, France, 2020.

[29] M. Antoniou, D. Tsounidi, P. S. Petrou, K. G. Beltsios, and S. E. Kakabakos, "Functionalization of silicon dioxide and silicon nitride surfaces with aminosilanes for optical biosensing applications," *Med. Devices Sensors*, vol. 3, no. 5, Oct. 2020, Art. no. e10072, doi: 10.1002/mds3.10072.

Abhijeet Barua received the B.Tech. degree in electrical engineering from the National Institute of Technology (NIT), Rourkela, India, in 2011, and the Ph.D. degree in electrical engineering and computer science as a member of the Microelectronics and Integrated-Systems With Neuro-Centric Devices (MIND) Laboratory, University of Cincinnati, in 2021. He is currently a Process Engineer with Intel Corporation, USA. His current research interests include amorphous oxide semiconductors, TFT, ferroelectric FET, RRAM, device physics, modeling, transistor performance, RTN, BTI, parasitic parameters, deposition techniques, and biosensor applications.

Ryan J. White received the B.S. degree in chemistry from the University of North Carolina in 2003 and the Ph.D. degree in chemistry from the University of Utah in 2007. He was an Assistant Professor of Chemistry and Biochemistry at UMBC in 2011 and was promoted to an Associate Professor with tenure in 2016. He joined UC in the fall of 2017. He is an Associate Professor and an Ohio Eminent Scholar with the University of Cincinnati with joint appointments in the Department of Chemistry and Electrical Engineering. His research group works on the development of specific chemical sensing and imaging platforms and the application of these platforms toward biomedical and biological applications. He was an NIH NRSA Postdoctoral Fellow at the University of California at Santa Barbara. He was a recipient of the Royce W. Murray Young Investigator Award from the Society for Electroanalytical Chemistry.

Kevin D. Leedy received the B.S. degree in metallurgical engineering from the University of Cincinnati in 1991 and the M.S. and Ph.D. degrees in metallurgical engineering from the University of Illinois at Urbana–Champaign in 1993 and 1997, respectively. He is a Senior Materials Research Engineer with the U.S. Air Force Research Laboratory, Sensors Directorate, Wright–Patterson Air Force Base, OH. He manages the Sensors Directorate Cleanroom. His research interests include metal oxide thin films and bulk crystals, transparent conductive oxides, dielectrics, thin film transistors, varactors, thin film resistors, memristors, plasmonics, phase change materials, pulsed laser deposition, atomic layer deposition, and sputtering.

Vidya Chidambaran received the M.B.B.S. degree from Bangalore University, India, and the M.D. degree in anesthesiology from Rajiv Gandhi University, India, with residency in Anesthesiology from Brookdale University, the Fellowship in pediatric anesthesia from Johns Hopkins University, and the master's degree in clinical and translational research from the University of Cincinnati. She has published more than 50 peer-reviewed articles in various international journals and more than 80 conference abstracts. Her research interests include personalized pain medicine, pharmacogenomics, epigenetics, chronic post-surgical pain, disparities, and psychosocial predictors of pain in children.

Rashmi Jha received the B.Tech. degree in electrical engineering from IIT Kharagpur, India, in 2000, and the M.S. and Ph.D. degrees in electrical engineering from North Carolina State University, Raleigh, North Carolina, USA, in 2003 and 2006, respectively. She worked as a Process Integration Engineer for advanced CMOS technologies at the IBM Semiconductor Research and Development Center, East Fishkill, NY, USA. She is a Professor with the Electrical Engineering and Computer Science (EECS) Department, University of Cincinnati, Cincinnati, USA. She holds 13 U.S. patents and has authored/coauthored several publications. Her current research interests include advanced CMOS and beyond CMOS devices, artificial intelligence, neuromorphic and brain-inspired SoC, cybersecurity with emphasis on microelectronics, and neuroelectronics. She was a recipient of the Summer Faculty Fellowship Award from AFOSR, USA, in 2021 and 2017, the CAREER Award from the National Science Foundation (NSF), USA, in 2013, the IBM Faculty Award in 2012, and the IBM Invention Achievement Award in 2007. She is the Director of Microelectronics and Integrated Computing Systems with the Neurocentric Devices (MIND) Laboratory, University of Cincinnati.